DESY–10–250
December 2010

Study of tau-pair production at HERA

ZEUS Collaboration

Abstract

A study of events containing two tau leptons with high transverse momentum has been performed with the ZEUS detector at HERA, using a data sample corresponding to an integrated luminosity of 0.33 fb^{-1}. The tau candidates were identified from their decays into electrons, muons or hadronic jets. The number of tau-pair candidates has been compared with the prediction from the Standard Model, where the largest contribution is expected from Bethe-Heitler processes. The total visible cross section was extracted. Standard Model expectations agree well with the measured distributions, also at high invariant mass of the tau pair.

The ZEUS Collaboration

H. Abramowicz[44,ag], L. Adamczyk[13], M. Adamus[53], R. Aggarwal[7,d], S. Antonelli[4], P. Antonioli[3], A. Antonov[32], M. Arneodo[49], V. Aushev[26], Y. Aushev[26,aa], O. Bachynska[15], A. Bamberger[19], A.N. Barakbaev[25], G. Barbagli[17], G. Bari[3], F. Barreiro[29], N. Bartosik[26,ab], D. Bartsch[5], M. Basile[4], O. Behnke[15], J. Behr[15], U. Behrens[15], L. Bellagamba[3], A. Bertolin[38], S. Bhadra[56], M. Bindi[4], C. Blohm[15], V. Bokhonov[26], T. Bołd[13], O. Bolilyi[26,ab], E.G. Boos[25], K. Borras[15], D. Boscherini[3], D. Bot[15], S.K. Boutle[51], I. Brock[5], E. Brownson[55], R. Brugnera[39], N. Brümmer[36], A. Bruni[3], G. Bruni[3], B. Brzozowska[52], P.J. Bussey[20], J.M. Butterworth[51], B. Bylsma[36], A. Caldwell[34], M. Capua[8], R. Carlin[39], C.D. Catterall[56], S. Chekanov[1], J. Chwastowski[12,f], J. Ciborowski[52,ak], R. Ciesielski[15,h], L. Cifarelli[4], F. Cindolo[3], A. Contin[4], A.M. Cooper-Sarkar[37], N. Coppola[15,i], M. Corradi[3], F. Corriveau[30], M. Costa[48], G. D'Agostini[42], F. Dal Corso[38], J. del Peso[29], R.K. Dementiev[33], S. De Pasquale[4,b], M. Derrick[1], R.C.E. Devenish[37], D. Dobur[19,u], B.A. Dolgoshein[32], G. Dolinska[26], A.T. Doyle[20], V. Drugakov[16], L.S. Durkin[36], S. Dusini[38], Y. Eisenberg[54], P.F. Ermolov [33,†], A. Eskreys[12], S. Fang[15,j], S. Fazio[8], J. Ferrando[37], M.I. Ferrero[48], J. Figiel[12], M. Forrest[20], B. Foster[37], S. Fourletov[50,w], G. Gach[13], A. Galas[12], E. Gallo[17], A. Garfagnini[39], A. Geiser[15], I. Gialas[21,x], L.K. Gladilin[33], D. Gladkov[32], C. Glasman[29], O. Gogota[26], Yu.A. Golubkov[33], P. Göttlicher[15,k], I. Grabowska-Bołd[13], J. Grebenyuk[15], I. Gregor[15], G. Grigorescu[35], G. Grzelak[52], O. Gueta[44], C. Gwenlan[37,ad], T. Haas[15], W. Hain[15], R. Hamatsu[47], J.C. Hart[43], H. Hartmann[5], G. Hartner[56], E. Hilger[5], D. Hochman[54], R. Hori[46], K. Horton[37,ae], A. Hüttmann[15], G. Iacobucci[3], Z.A. Ibrahim[10], Y. Iga[41], R. Ingbir[44], M. Ishitsuka[45], H.-P. Jakob[5], F. Januschek[15], M. Jimenez[29], T.W. Jones[51], M. Jüngst[5], I. Kadenko[26], B. Kahle[15], B. Kamaluddin [10,†], S. Kananov[44], T. Kanno[45], U. Karshon[54], F. Karstens[19,v], I.I. Katkov[15,l], M. Kaur[7], P. Kaur[7,d], A. Keramidas[35], L.A. Khein[33], J.Y. Kim[9], D. Kisielewska[13], S. Kitamura[47,ai], R. Klanner[22], U. Klein[15,m], E. Koffeman[35], P. Kooijman[35], Ie. Korol[26], I.A. Korzhavina[33], A. Kotański[14,g], U. Kötz[15], H. Kowalski[15], P. Kulinski[52], O. Kuprash[26,ac], M. Kuze[45], A. Lee[36], B.B. Levchenko[33], A. Levy[44], V. Libov[15], S. Limentani[39], T.Y. Ling[36], M. Lisovyi[15], E. Lobodzinska[15], W. Lohmann[16], B. Löhr[15], E. Lohrmann[22], J.H. Loizides[51], K.R. Long[23], A. Longhin[38], D. Lontkovskyi[26,ac], O.Yu. Lukina[33], P. Łużniak[52,al], J. Maeda[45,ah], S. Magill[1], I. Makarenko[26,ac], J. Malka[52,al], R. Mankel[15], A. Margotti[3], G. Marini[42], J.F. Martin[50], A. Mastroberardino[8], M.C.K. Mattingly[2], I.-A. Melzer-Pellmann[15], S. Mergelmeyer[5], S. Miglioranzi[15,n], F. Mohamad Idris[10], V. Monaco[48], A. Montanari[15], J.D. Morris[6,c], K. Mujkic[15,o], B. Musgrave[1], K. Nagano[24], T. Namsoo[15,p], R. Nania[3], D. Nicholass[1,a], A. Nigro[42], Y. Ning[11], U. Noor[56], D. Notz[15], R.J. Nowak[52], A.E. Nuncio-Quiroz[5], B.Y. Oh[40], N. Okazaki[46], K. Oliver[37], K. Olkiewicz[12], Yu. Onishchuk[26], K. Papageorgiu[21], A. Parenti[15], E. Paul[5], J.M. Pawlak[52], B. Pawlik[12], P. G. Pelfer[18], A. Pellegrino[35], W. Perlanski[52,al], H. Perrey[22], K. Piotrzkowski[28], P. Plucinski[53,am], N.S. Pokrovskiy[25], A. Polini[3], A.S. Proskuryakov[33], M. Przybycień[13], A. Raval[15], D.D. Reeder[55], B. Reisert[34], Z. Ren[11], J. Repond[1], Y.D. Ri[47,aj], A. Robertson[37], P. Roloff[15], E. Ron[29], I. Rubinsky[15], M. Ruspa[49], R. Sacchi[48], A. Salii[26], U. Samson[5], G. Sartorelli[4], A.A. Savin[55], D.H. Saxon[20], M. Schioppa[8], S. Schlenstedt[16], P. Schleper[22], W.B. Schmidke[34], U. Schneekloth[15], V. Schönberg[5], T. Schörner-Sadenius[15], J. Schwartz[30],

F. Sciulli[11], L.M. Shcheglova[33], R. Shehzadi[5], S. Shimizu[46,n], I. Singh[7,d], I.O. Skillicorn[20], W. Słomiński[14], W.H. Smith[55], V. Sola[48], A. Solano[48], D. Son[27], V. Sosnovtsev[32], A. Spiridonov[15,q], H. Stadie[22], L. Stanco[38], A. Stern[44], T.P. Stewart[50], A. Stifutkin[32], P. Stopa[12], S. Suchkov[32], G. Susinno[8], L. Suszycki[13], J. Sztuk-Dambietz[22], D. Szuba[15,r], J. Szuba[15,s], A.D. Tapper[23], E. Tassi[8,e], J. Terrón[29], T. Theedt[15], H. Tiecke[35], K. Tokushuku[24,y], O. Tomalak[26], J. Tomaszewska[15,t], T. Tsurugai[31], M. Turcato[22], T. Tymieniecka[53,an], C. Uribe-Estrada[29], M. Vázquez[35,n], A. Verbytskyi[15], O. Viazlo[26], N.N. Vlasov[19,w], O. Volynets[26], R. Walczak[37], W.A.T. Wan Abdullah[10], J.J. Whitmore[40,af], J. Whyte[56], L. Wiggers[35], M. Wing[51], M. Wlasenko[5], G. Wolf[15], H. Wolfe[55], K. Wrona[15], A.G. Yagües-Molina[15], S. Yamada[24], Y. Yamazaki[24,z], R. Yoshida[1], C. Youngman[15], A.F. Żarnecki[52], L. Zawiejski[12], O. Zenaiev[26], W. Zeuner[15,n], B.O. Zhautykov[25], N. Zhmak[26,aa], C. Zhou[30], A. Zichichi[4], M. Zolko[26], D.S. Zotkin[33], Z. Zulkapli[10]

[1] *Argonne National Laboratory, Argonne, Illinois 60439-4815, USA* [A]
[2] *Andrews University, Berrien Springs, Michigan 49104-0380, USA*
[3] *INFN Bologna, Bologna, Italy* [B]
[4] *University and INFN Bologna, Bologna, Italy* [B]
[5] *Physikalisches Institut der Universität Bonn, Bonn, Germany* [C]
[6] *H.H. Wills Physics Laboratory, University of Bristol, Bristol, United Kingdom* [D]
[7] *Panjab University, Department of Physics, Chandigarh, India*
[8] *Calabria University, Physics Department and INFN, Cosenza, Italy* [B]
[9] *Institute for Universe and Elementary Particles, Chonnam National University, Kwangju, South Korea*
[10] *Jabatan Fizik, Universiti Malaya, 50603 Kuala Lumpur, Malaysia* [E]
[11] *Nevis Laboratories, Columbia University, Irvington on Hudson, New York 10027, USA* [F]
[12] *The Henryk Niewodniczanski Institute of Nuclear Physics, Polish Academy of Sciences, Cracow, Poland* [G]
[13] *Faculty of Physics and Applied Computer Science, AGH-University of Science and Technology, Cracow, Poland* [H]
[14] *Department of Physics, Jagellonian University, Cracow, Poland*
[15] *Deutsches Elektronen-Synchrotron DESY, Hamburg, Germany*
[16] *Deutsches Elektronen-Synchrotron DESY, Zeuthen, Germany*
[17] *INFN Florence, Florence, Italy* [B]
[18] *University and INFN Florence, Florence, Italy* [B]
[19] *Fakultät für Physik der Universität Freiburg i.Br., Freiburg i.Br., Germany*
[20] *School of Physics and Astronomy, University of Glasgow, Glasgow, United Kingdom* [D]
[21] *Department of Engineering in Management and Finance, Univ. of the Aegean, Chios, Greece*
[22] *Hamburg University, Institute of Experimental Physics, Hamburg, Germany* [I]
[23] *Imperial College London, High Energy Nuclear Physics Group, London, United Kingdom* [D]
[24] *Institute of Particle and Nuclear Studies, KEK, Tsukuba, Japan* [J]
[25] *Institute of Physics and Technology of Ministry of Education and Science of Kazakhstan, Almaty, Kazakhstan*
[26] *Institute for Nuclear Research, National Academy of Sciences, and National University of Kyiv, Kyiv, Ukraine"*
[27] *Kyungpook National University, Center for High Energy Physics, Daegu, South Korea* [K]
[28] *Institut de Physique Nucléaire, Université Catholique de Louvain, Louvain-la-Neuve, Belgium* [L]
[29] *Departamento de Física Teórica, Universidad Autónoma de Madrid, Madrid, Spain* [M]
[30] *Department of Physics, McGill University, Montréal, Québec, Canada H3A 2T8* [N]
[31] *Meiji Gakuin University, Faculty of General Education, Yokohama, Japan* [J]
[32] *Moscow Engineering Physics Institute, Moscow, Russia* [O]

[33] *Moscow State University, Institute of Nuclear Physics, Moscow, Russia* [P]
[34] *Max-Planck-Institut für Physik, München, Germany*
[35] *NIKHEF and University of Amsterdam, Amsterdam, Netherlands* [Q]
[36] *Physics Department, Ohio State University, Columbus, Ohio 43210, USA* [A]
[37] *Department of Physics, University of Oxford, Oxford, United Kingdom* [D]
[38] *INFN Padova, Padova, Italy* [B]
[39] *Dipartimento di Fisica dell' Università and INFN, Padova, Italy* [B]
[40] *Department of Physics, Pennsylvania State University, University Park, Pennsylvania 16802, USA* [F]
[41] *Polytechnic University, Sagamihara, Japan* [J]
[42] *Dipartimento di Fisica, Università 'La Sapienza' and INFN, Rome, Italy* [B]
[43] *Rutherford Appleton Laboratory, Chilton, Didcot, Oxon, United Kingdom* [D]
[44] *Raymond and Beverly Sackler Faculty of Exact Sciences, School of Physics, Tel Aviv University, Tel Aviv, Israel* [R]
[45] *Department of Physics, Tokyo Institute of Technology, Tokyo, Japan* [J]
[46] *Department of Physics, University of Tokyo, Tokyo, Japan* [J]
[47] *Tokyo Metropolitan University, Department of Physics, Tokyo, Japan* [J]
[48] *Università di Torino and INFN, Torino, Italy* [B]
[49] *Università del Piemonte Orientale, Novara, and INFN, Torino, Italy* [B]
[50] *Department of Physics, University of Toronto, Toronto, Ontario, Canada M5S 1A7* [N]
[51] *Physics and Astronomy Department, University College London, London, United Kingdom* [D]
[52] *Faculty of Physics, University of Warsaw, Warsaw, Poland*
[53] *Institute for Nuclear Studies, Warsaw, Poland*
[54] *Department of Particle Physics and Astrophysics, Weizmann Institute, Rehovot, Israel*
[55] *Department of Physics, University of Wisconsin, Madison, Wisconsin 53706, USA* [A]
[56] *Department of Physics, York University, Ontario, Canada M3J 1P3* [N]

[A] supported by the US Department of Energy
[B] supported by the Italian National Institute for Nuclear Physics (INFN)
[C] supported by the German Federal Ministry for Education and Research (BMBF), under contract No. 05 H09PDF
[D] supported by the Science and Technology Facilities Council, UK
[E] supported by an FRGS grant from the Malaysian government
[F] supported by the US National Science Foundation. Any opinion, findings and conclusions or recommendations expressed in this material are those of the authors and do not necessarily reflect the views of the National Science Foundation.
[G] supported by the Polish Ministry of Science and Higher Education as a scientific project No. DPN/N188/DESY/2009
[H] supported by the Polish Ministry of Science and Higher Education as a scientific project (2009-2010)
[I] supported by the German Federal Ministry for Education and Research (BMBF), under contract No. 05h09GUF, and the SFB 676 of the Deutsche Forschungsgemeinschaft (DFG)
[J] supported by the Japanese Ministry of Education, Culture, Sports, Science and Technology (MEXT) and its grants for Scientific Research
[K] supported by the Korean Ministry of Education and Korea Science and Engineering Foundation
[L] supported by FNRS and its associated funds (IISN and FRIA) and by an Inter-University Attraction Poles Programme subsidised by the Belgian Federal Science Policy Office
[M] supported by the Spanish Ministry of Education and Science through funds provided by CICYT
[N] supported by the Natural Sciences and Engineering Research Council of Canada (NSERC)
[O] partially supported by the German Federal Ministry for Education and Research (BMBF)
[P] supported by RF Presidential grant N 41-42.2010.2 for the Leading Scientific Schools and by the Russian Ministry of Education and Science through its grant for Scientific Research on High Energy Physics
[Q] supported by the Netherlands Foundation for Research on Matter (FOM)
[R] supported by the Israel Science Foundation

[a] also affiliated with University College London, United Kingdom
[b] now at University of Salerno, Italy
[c] now at Queen Mary University of London, United Kingdom
[d] also funded by Max Planck Institute for Physics, Munich, Germany
[e] also Senior Alexander von Humboldt Research Fellow at Hamburg University, Institute of Experimental Physics, Hamburg, Germany
[f] also at Cracow University of Technology, Faculty of Physics, Mathemathics and Applied Computer Science, Poland
[g] supported by the research grant No. 1 P03B 04529 (2005-2008)
[h] now at Rockefeller University, New York, NY 10065, USA
[i] now at DESY group FS-CFEL-1
[j] now at Institute of High Energy Physics, Beijing, China
[k] now at DESY group FEB, Hamburg, Germany
[l] also at Moscow State University, Russia
[m] now at University of Liverpool, United Kingdom
[n] now at CERN, Geneva, Switzerland
[o] also affiliated with Universtiy College London, UK
[p] now at Goldman Sachs, London, UK
[q] also at Institute of Theoretical and Experimental Physics, Moscow, Russia
[r] also at INP, Cracow, Poland
[s] also at FPACS, AGH-UST, Cracow, Poland
[t] partially supported by Warsaw University, Poland
[u] now at Istituto Nucleare di Fisica Nazionale (INFN), Pisa, Italy
[v] now at Haase Energie Technik AG, Neumünster, Germany
[w] now at Department of Physics, University of Bonn, Germany
[x] also affiliated with DESY, Germany
[y] also at University of Tokyo, Japan
[z] now at Kobe University, Japan
[†] deceased
[aa] supported by DESY, Germany
[ab] member of National University of Kyiv - Mohyla Academy, Kyiv, Ukraine
[ac] supported by the Bogolyubov Institute for Theoretical Physics of the National Academy of Sciences, Ukraine
[ad] STFC Advanced Fellow
[ae] nee Korcsak-Gorzo
[af] This material was based on work supported by the National Science Foundation, while working at the Foundation.
[ag] also at Max Planck Institute for Physics, Munich, Germany, External Scientific Member
[ah] now at Tokyo Metropolitan University, Japan
[ai] now at Nihon Institute of Medical Science, Japan
[aj] now at Osaka University, Osaka, Japan

[ak] also at Łódź University, Poland
[al] member of Łódź University, Poland
[am] now at Lund University, Lund, Sweden
[an] also at University of Podlasie, Siedlce, Poland

1 Introduction

The production of isolated-lepton pairs at the *ep* collider HERA is dominated by the two-photon Bethe-Heitler process, $\gamma\gamma \to l^+l^-$, and can be accurately predicted in the Standard Model (SM) [1]. Possible deviations of the event yield or final-state distributions from the prediction of the SM could be a hint for new physics. The measurement of multi-lepton production at HERA attracted some interest, especially after the observation of an excess of events at high mass in multi-electron final states, observed by the H1 Collaboration in the HERA I (1994–2000) data [2]. Recently, the H1 and ZEUS Collaborations have published [3–5] a study of multi-electron and multi-muon events based on the entire statistics collected at HERA. Further investigations of multi-lepton events were performed in tau-pair production by H1 [6], based on the HERA I data.

This paper reports a study of ditau events with the ZEUS detector, with data collected in the HERA II running phase (2004–2007). The taus are identified from their decay into an electron, a muon or a hadronic jet. The hadronic channel is selected with a technique analogous to that used in a previous ZEUS publication on single-tau production [7], where two interesting events, with a high-transverse-energy tau candidate and large missing transverse momentum, were observed in the HERA I data.

2 Experimental set-up

The data were collected between 2004 and 2007 at the *ep* collider HERA using the ZEUS detector. During this period HERA operated with an electron or positron[1] beam with an energy of 27.5 GeV and a proton beam with an energy of 920 GeV. The e^-p data correspond to an integrated luminosity of 179 pb^{-1}, while the e^+p collisions correspond to 155 pb^{-1}, giving a total of 334 pb^{-1}. The lepton beams were polarised, with roughly equal periods for right-handed and left-handed polarisation, such that the average polarisation was negligible.

A detailed description of the ZEUS detector can be found elsewhere [8]. A brief outline of the components that are most relevant for this analysis is given below.

Charged particles were tracked in the central tracking detector (CTD) [9], which operated in a magnetic field of 1.43 T provided by a thin superconducting solenoid. The CTD consisted of 72 cylindrical drift chamber layers, organised in nine superlayers covering the

[1] Here and in the following, the term "electron" denotes generically both the electron (e^-) and the positron (e^+), unless otherwise specified.

polar-angle[2] region $15^\circ < \theta < 164^\circ$. The CTD was complemented by a silicon microvertex detector (MVD) [10], consisting of three active layers in the barrel and four disks in the forward region.

The high-resolution uranium–scintillator calorimeter (CAL) [11] consisted of three parts: the forward (FCAL), the barrel (BCAL) and the rear (RCAL) calorimeters. Each part was subdivided transversely into towers and longitudinally into one electromagnetic section (EMC) and either one (in RCAL) or two (in BCAL and FCAL) hadronic sections (HAC). The smallest subdivision of the calorimeter was called a cell. The CAL energy resolutions, as measured under test-beam conditions, were $\sigma(E)/E = 0.18/\sqrt{E}$ for electrons and $\sigma(E)/E = 0.35/\sqrt{E}$ for hadrons, with E in GeV.

The muon system consisted of barrel, rear (B/RMUON) [8] and forward (FMUON) tracking detectors. The BMUON (RMUON) consisted of limited-streamer (LS) tube chambers placed behind the BCAL (RCAL), inside and outside a magnetised iron yoke surrounding the CAL, covering the polar-angle region $34^\circ < \theta < 135^\circ$ ($135^\circ < \theta < 171^\circ$). The FMUON consisted of six trigger planes of LS tubes and four planes of drift chambers covering the polar-angle region $5^\circ < \theta < 32^\circ$.

The luminosity was measured using the Bethe-Heitler reaction $ep \to e\gamma p$ by a luminosity detector which consisted of a lead–scintillator calorimeter [12] and an independent magnetic spectrometer [13]. The fractional uncertainty on the measured luminosity was 1.9%.

3 Signal and background processes

The signal considered in this analysis is the presence of two isolated taus at high transverse energy from the reaction $ep \to (e)\tau^+\tau^- X$. The scattered electron is observed in the calorimeter only for high virtuality of the photon at the electron vertex, Q^2. The proton either stays intact (elastic reaction, $X = p$) or dissociates into a resonant (quasi-elastic) or hadronic system (inelastic). In order to suppress the dominant backgrounds from deep inelastic scattering (DIS) neutral current (NC), $ep \to eX$, and photoproduction, $\gamma p \to X$, only events where no deposit was observed in the forward part of the calorimeter were selected. The dominant signal process ($\simeq 71\%$ estimated from Monte Carlo simulation after all selection cuts) was therefore the elastic reaction $ep \to (e)p\tau^+\tau^-$, where the final-state proton stays intact. The quasi-elastic reaction was the second most important

[2] The ZEUS coordinate system is a right-handed Cartesian system, with the Z axis pointing in the proton beam direction, referred to as the "forward direction", and the X axis pointing left towards the centre of HERA. The polar angle, θ, is measured with respect to the proton beam direction. The coordinate origin is at the nominal interaction point.

contribution ($\simeq 27\%$). In this case the final-state proton dissociates into a system with small invariant mass, escaping in the forward beam pipe. The contribution of events $ep \to e\tau^+\tau^- X$, in which the scattered electron was observed in the calorimeter, was determined to be only $\simeq 1\%$ after all analysis cuts.

The two tau leptons were identified from their decays into an electron, a muon or hadrons, respectively, resulting in the final-state signatures listed in Table 1. The topologies in which the two tau leptons both decayed into either electrons or muons were not considered, due to the irreducible background of dielectron and dimuon processes. Hadronic decays give rise to narrow and low-multiplicity jets; these characteristics allowed tau decays to be distinguished from the much more abundant QCD-induced jets, as described in Section 4.3.

Monte Carlo (MC) programs were used to generate the signal and background events in order to optimise the selection cuts and determine acceptances.

The GRAPE event generator [14] was used to simulate signal events. It is based on the exact electroweak matrix elements in photon-photon (and also photon-Z^0 and Z^0-Z^0) collisions and internal photon or Z^0 conversions at tree level. The three contributions at the proton vertex, elastic, quasi-elastic and inelastic, were generated separately. The cross section for tau-pair production falls steeply with the transverse energy of the tau lepton.

Dielectron events $ep \to (e)e^+e^-X$ were a potential background especially to the topology (e-)e-jet and were also generated with the GRAPE program. Dimuon events, which represented the main background to the (e-)e-μ and (e-)μ-jet final states, were also generated with GRAPE.

Due to the requirement that the events be (quasi-)elastic, the main background to the hadronic channel consisted of diffractive dijet production. Diffractive DIS production, which was the main background to the topologies (e-)jet-jet and (e-)e-jet, was generated with the RAPGAP [15] program. The same program was used to generate diffractive dijet events in the photoproduction regime, both in resolved and direct photon processes, which represented the main background to the jet-jet topology. Since the MC events did not adequately describe the data distributions, the resolved and direct contributions were separately normalised to the data using an independent sample from that used in the analysis (see Section 4.4). Non-diffractive DIS and photoproduction events were generated with the DJANGOH [16] and PYTHIA [17] programs, respectively.

The generated events were passed through the GEANT 3.21-based [18] ZEUS detector- and trigger-simulation programs. They were reconstructed and analysed using the same program chain as the data.

4 Event selection

The events were selected online by the ZEUS three-level trigger system [8, 19], using a combination of several trigger chains which required typically either the presence of hadronic jets, an electron or a muon in the final state. The trigger requirements were looser than the offline selection. The offline selection proceeded in two steps [20]. A preselection required low track multiplicity and no energy around the beam-pipe hole in the forward region of the detector, as expected for (quasi-)elastic ditau production. A second step required the presence of at least two objects among electrons, muons or jets, identified as the tau decays, and classified the events in the categories listed in Table 1. This selection is described in more detail below.

4.1 Preselection

The following offline criteria were imposed at preselection level:

- the number of good tracks in the event, $N_{\rm trk}$, was required to be at least 2 and at most 7, as expected for the ditau topologies studied. A good track was defined to pass through at least 3 CTD superlayers, to have hits in the MVD or in the innermost CTD superlayer and to have a transverse momentum greater than 150 MeV;

- the Z coordinate of the interaction vertex, reconstructed using tracks, was restricted to $|Z_{\rm VTX}| < 40$ cm in order to reject the background due to non-ep interactions;

- the energy $E^{\rm IR}_{\rm FCAL}$, reconstructed from the sum of the energy deposits in the CAL cells in the first inner ring around the forward beam-pipe hole, was restricted to be less than 1 GeV in order to select (quasi-)elastic events;

- the $E - P_Z$ of the final state, reconstructed from the sum of the total and longitudinal energy deposits of the cells in the calorimeter, was required to be less than 60 GeV. For events with a muon, the $(E - P_Z)$ of the CAL deposit associated with the muon was replaced by that of the muon track. For fully contained events, $E - P_Z$ is twice the electron-beam energy and peaks at 55 GeV. This requirement rejected ep interactions overlapping with background events.

Other selection criteria were applied to reject residual non-ep interactions, mainly beam-gas events and cosmic rays. It was verified that the loss of signal events due to these cuts was negligible.

4.2 Identification of electrons and muons

An algorithm which combined information from the energy deposits in the calorimeter with tracks [21] was used to identify possible electron candidates. The electron four-momenta were reconstructed from the CAL. The electron candidates were required to have a transverse energy $p_T^e > 2$ GeV, to be in the polar-angle range $17^\circ < \theta_e < 160^\circ$ and to have a good track matched to the calorimeter deposit. The matched track was required to have an extrapolated distance of closest approach to the calorimeter deposit of less than 8 cm. The electron candidate was required to be isolated such that the total energy not associated with the electron in an η-ϕ cone of radius 0.8 centred on the electron direction, where ϕ is the azimuthal angle and η is the pseudorapidity, was less than 2 GeV. This requirement was complemented by the requirement that no track, other than the matching track, was contained in an η-ϕ cone of radius 1 centred on the electron direction. Further fiducial cuts [20] were applied in the RCAL to guarantee that the experimental acceptance was well understood. The charge of the track matched to the electron, Q_e, was also used to discriminate the signal from the background. The track charge information was used only if its significance $S^{\rm trk} = |Q/r|/\sigma(Q/r)$ was greater than 1.5, where r denotes the radius of the track helix and σ is the uncertainty.

The muons were required to be reconstructed in the rear or barrel muon chambers and to be matched to a good track and to a calorimeter deposit. The muon transverse momentum and direction were reconstructed from the matched track. Each muon candidate was required to have a transverse momentum $p_T^\mu > 2$ GeV and to lie in the angular region $34^\circ < \theta_\mu < 157^\circ$. The muon was required to be isolated such that only the matching track was contained in an η-ϕ cone of radius 1 centred on the muon direction. If a second muon candidate, reconstructed with looser criteria, was found in the event, this event was rejected.

4.3 Identification of hadronic tau decays

The jets deriving from the hadronic tau decay were reconstructed from the CAL cells using the k_T cluster algorithm [22] in the longitudinally invariant inclusive mode [23], assuming massless objects, and were corrected for energy loss due to the dead material in front of the CAL. The jets were required to have a transverse energy $E_T^{\rm jet} > 5$ GeV and pseudorapidity $|\eta^{\rm jet}| < 2$. At least one good track associated with the jet was required in an η-ϕ cone of radius 1 around the jet axis. The fraction $f_{\rm EMC}$ of the jet energy in the electromagnetic section of the calorimeter was required to satisfy $f_{\rm EMC} < \min(0.95, 2 \cdot R_{90\%} + 0.7)$, where $R_{90\%}$ is the radius of the η-ϕ cone centred on the jet axis that contains 90% of the jet energy. These two cuts rejected electrons faking hadronic tau decays. Further fiducial

cuts [20] were applied on the jet direction in order to exclude regions of the CAL where the jet energy was not precisely measured.

Jets originating from hadronic tau decays are characterised by their low mass, low multiplicity (mostly either one or three tracks) and pencil-like shape. In contrast, QCD-induced hadronic jets are typically broader and have higher multiplicity. These properties were exploited to discriminate tau jets from QCD jets using a multi-variate discrimination technique [24] which was used in a previous publication [7]. The jet shape was characterised by six variables. Five of these variables were the same as those used in previous analyses [7, 25]: the first and the second moment of the radial extension of the jet-energy deposition ($R_{\rm mean}$ and $R_{\rm rms}$, respectively); the first moment of the energy deposition in the direction along the jet axis ($L_{\rm mean}$); the number of subjets within the jet resolved with a resolution criterion $y_{\rm cut}$ [26] of $5 \cdot 10^{-4}$ ($N_{\rm subj}$); and the mass of the jet calculated from the CAL cells associated with the jet ($M_{\rm jet}$). The sixth variable, which was used for this analysis, was the sum of the distances in the η-ϕ plane between the jet axis and the tracks associated with the jet, $R_{\rm trk} = \sum_i^{\rm N_{trk}} \sqrt{(\Delta\eta_i^2 + \Delta\phi_i^2)}$.

The six variables were combined in a discriminant $\mathcal{D}$ given, for each point in the phase space $\vec{x}(-\log(R_{\rm mean}), -\log(R_{\rm rms}), -\log(1 - L_{\rm mean}), N_{\rm subj}, M_{\rm jet}, \log(R_{\rm trk}))$, by:

$$\mathcal{D}(\vec{x}) = \frac{\rho_{\rm sig}(\vec{x})}{\rho_{\rm sig}(\vec{x}) + \rho_{\rm bkg}(\vec{x})},$$

where $\rho_{\rm sig}$ and $\rho_{\rm bkg}$ are the density functions of the signal and the background, respectively. The densities were calculated from a method based on range searching [24] and were determined from a sample of single-tau MC events for the signal and DJANGOH DIS NC events for the background. For any given jet with phase-space coordinate $\vec{x}$, the signal and the background densities were evaluated from the number of corresponding simulated signal and background jets in a 6-dimensional box of fixed size centred around $\vec{x}$.

Figure 1 shows the six discriminant variables for the data, compared to those of the sum of the MC expectations, where all cuts described in this Section, except the discriminant cut, were applied. The MC agrees well with the data, both in shape and in normalisation. The discriminant variable is shown in Fig. 2 for each jet in each decay channel. As expected, the ditau signal MC dominates at large values of $\mathcal{D}$, while the background from the other processes populates the lower values of $\mathcal{D}$. In order to select the hadronic tau decays, a cut on the discriminant greater than 0.8 was applied on each tau-candidate jet.

4.4 Final selection

After the preselection cuts, the possible decay products of each tau were searched for and the final state was classified in the eight exclusive topologies listed in Table 1, in which

each tau of the pair could decay into an electron, a muon, or a hadronic jet. For high Q^2, the scattered electron could also be observed in the CAL, giving an additional electron in the topology. For lower Q^2, the scattered electron escaped down the beam pipe in the electron-beam direction. In this case, the quantity $E - P_Z$ is typically much less than 55 GeV and a cut, $E - P_Z < 45$ GeV, was applied to reduce the DIS NC background.

The following additional cuts, also listed in Table 1, were applied in each case:

- in the (e-)e-μ topology, exactly one muon, (two) one electron(s) and no additional tracks were required in the final state. In the e-μ topology, the electron charge, Q_e, was required to be opposite to that of the muon track, Q_μ. In addition, in order to reduce the main background due to dimuon production at high Q^2, where one of the muons was outside the acceptance of the detector, the electron was required to have charge opposite to that of the electron beam, $Q_{\rm beam}$, if $\theta_e > 1.0$ and $S^{\rm trk} > 1.5$;
- in the (e-)e-jet channel, (two) one electron(s) were required in the event together with exactly one tau-candidate jet. In the e-jet channel, the cuts on the electron were the same as in the e-μ channel, in order to reject the dominant background due to DIS NC events $ep \to eX$. In addition, the charge $Q_{\rm jet} = \sum_i Q_{i,{\rm trk}}$ was reconstructed for the jet, summing the charges $Q_{i,{\rm trk}}$ of all tracks, with significance $S^{\rm trk} > 1.5$, associated with the jet. If all tracks satisfied the $S^{\rm trk}$ criterion, the jet charge was required to be $Q_{\rm jet} = \pm 1$ and to be opposite to that of the electron candidate, as expected in the production of a tau pair;
- in the (e-)μ-jet topology, exactly (one electron) one muon and one tau-candidate jet were required to be present;
- for the (e-)jet-jet topology, exactly two candidate jets, and in the high-Q^2 topology an additional electron, were required. The jet-jet channel was dominated by the diffractive photoproduction dijet background and, in order to suppress it, the charge $Q_{\rm jet}$ was required to be ± 1 with the two jets having opposite charges. The $S^{\rm trk}$ requirement was the same as in the e-jet channel.

In total, 25 events were selected. Figure 3 shows the $E - P_Z$ distribution for the events and the distributions of the transverse momentum of the electron, muon and jet candidates, compared to the sum of the signal and background expectations.

All MC background expectations were normalised to the data luminosity, except the resolved and direct photoproduction contributions, both diffractive and non-diffractive. These four contributions were fitted to the data using two variables [20], which helped to distinguish the different processes: $x_\gamma^{\rm obs}$, which is an estimator of the fraction of photon's momentum taking part in the hard interaction; and $x_{I\!P}^{\rm obs}$, an estimator of the fraction of longitudinal momentum transferred from the proton in diffractive events. The four normalisation factors were determined in two steps and for this purpose an independent

data sample was used, which required the presence of two jets, $E - P_Z < 40$ GeV and $8 \leq N_{\rm trk} \leq 17$. The relative normalisation of the diffractive and non-diffractive MC contributions was determined first from a fit to the data of the $x_{I\!P}^{\rm obs}$ distribution for $x_\gamma^{\rm obs} < 0.5$. The four MC components were then fitted to the data $x_\gamma^{\rm obs}$ variable. The resulting normalisation factors were around 2, with an uncertainty of 25% and 15% for the diffractive and non-diffractive processes, respectively.

As shown in Fig. 3, the MC gives a good description of the data, both in shape and normalisation. The diffractive DIS dijet process is the main background in the e-jet-jet channel, while the diffractive photoproduction dijet process is the main background in the jet-jet channel. The dimuon production process is the main background to the topologies with a muon in the final state. In the e-jet topology, both the dielectron and the DIS diffractive processes contribute to the background.

4.5 Systematic uncertainties

The following sources of systematic uncertainties were considered (the resulting uncertainty on the total cross section is given in parentheses):

- the electron energy scale was changed by its uncertainty of 2% ($^{+0.2}_{-1.5}$%);
- the hadronic jet energy scale was varied by its uncertainty of 3% ($^{+26}_{-7}$%);
- the normalisation of the direct and resolved photoproduction background contributions, diffractive and non-diffractive, gave one of the main contributions to the uncertainty of the MC background expectation. The diffractive and non-diffractive normalisation factors were changed by their uncertainty of 25% and 15%, respectively ($\pm$11%);
- the total muon acceptance, including the trigger, the reconstruction and the muon identification efficiencies, is known to about 7% [4] ($\pm$4%);
- the cut on the track charge significance, $S^{\rm trk}$, was varied by ± 0.5 ($^{-12}_{-7}$%);
- the cut on the energy in the inner ring of the FCAL was varied ($^{+6}_{-12}$%);
- in the (e)-μ-jet channel, in order to account for the observed discrepancy in the discriminant distribution (see Fig. 2b), the Bethe-Heitler background was increased by 80% ($-$6%);
- the effect of potential differences between data and MC in the single-track efficiency [27], *e.g.*, from secondary interactions in the detector material, was evaluated (+5%);
- the overall normalisation uncertainty associated with the luminosity measurement was added ($\pm$1.9%);

- the statistical uncertainty of the few MC events that survive the cuts was added to the statistical uncertainty in the cross section.

A further check was performed on the tau-jet discriminant value. The $\rho_{\rm bkg}$ density used to determine $\mathcal{D}$ was calculated using as background the following different MC samples: the diffractive DIS dijet MC, the diffractive photoproduction dijet sample and the inclusive DIS NC Monte Carlo events. All samples gave very consistent values of the signal efficiency and background rejection, giving confidence in the method.

The total systematic uncertainty was obtained by adding the above contributions in quadrature, separately for the positive and negative deviations.

5 Results

The total selected number of ditau candidates, $N_{\rm data}$, is 25, of which 13 were selected in e^+p and 12 in e^-p collision data, consistent with the respective integrated luminosities. The total MC expectation was $34.8^{+3.9}_{-3.8}$ events, including an expected background, $N_{\rm bkg}$, of 11.6 ± 3.9 events (Table 2). The expected purity of the sample, evaluated from the GRAPE ditau and the background MC, was 67%. The number of selected events in each channel is shown in Table 2. One of the events in the jet-jet channel is shown in Fig. 4.

Figure 5 shows the visible invariant mass, $M_{\tau\tau}^{\rm visible}$, calculated from the two tau candidates, and the scalar sum of the visible transverse momenta of the two tau candidates in the event, $\sum p_{T,\tau\tau}^{\rm visible}$. No event with a visible mass $M_{\tau\tau}^{\rm visible}$ greater than 50 GeV was observed: the highest visible-mass candidate, found in the e-μ topology, had $M_{\tau\tau}^{\rm visible} = 49$ GeV. The MC predictions describe the data well and no excess is observed in the high-mass or high-$\sum p_{T,\tau\tau}^{\rm visible}$ region. Only one of the 25 data events had three objects, corresponding to an event with the scattered electron candidate in the detector, belonging to the e-e-jet topology.

The total cross section for ditau production was calculated for the kinematic region defined by $p_T^{\tau_{1,2}} > 5$ GeV and $17^\circ < \theta^{\tau_{1,2}} < 160^\circ$, where p_T^τ and θ^τ refer to the transverse momentum and polar angle, respectively, of the tau lepton. The cross section was calculated as

$$\sigma_{\tau\tau}^{\rm kin} = \frac{(N_{\rm data} - N_{\rm bkg})}{\mathcal{A} \cdot \mathcal{L}},$$

where $\mathcal{L}$ is the integrated luminosity of the data sample. The acceptance $\mathcal{A}$ was evaluated from the GRAPE ditau generator to be 1.23%. The total cross section was found to be

$$\sigma_{\tau\tau}^{\rm kin} = 3.3 \pm 1.3({\rm stat.})^{+1.0}_{-0.7}({\rm syst.})\ {\rm pb},$$

where the first uncertainty represents the statistical error and the second the systematic uncertainty. The cross-section value is in reasonable agreement with the SM expectation of $\sigma_{\tau\tau}^{\rm SM} = 5.67 \pm 0.16$ pb, as evaluated from the GRAPE MC generator.

6 Conclusions

Events with two tau candidates with high transverse momentum have been selected by the ZEUS experiment in the HERA II data and compared with the predictions of the Standard Model. The tau leptons were identified through their decays into electrons, muons or jets, with transverse momentum greater than 2 GeV (for an e or a μ) or 5 GeV (for a jet). The jet coming from the hadronic tau decay was identified with a multi-variate discrimination technique employed to separate the signal from the QCD background. The selected events were dominated by the Bethe-Heitler $\gamma\gamma \to \tau^+\tau^-$ process and the final-state topologies (e-)jet-jet, (e-)e-jet, (e-)e-μ and (e-)μ-jet were considered. In total, 25 events were selected, compared to a MC expectation of $34.8^{+3.9}_{-3.8}$ events, including 11.6 ± 3.9 events of expected background. The distribution of events shows good agreement with the Standard Model expectation, also at high values of the visible transverse momentum and visible invariant mass of the tau pair. Therefore, no evidence of physics beyond the Standard Model is found for tau-pair production. The total cross section, in the kinematic region $p_T^{\tau_{1,2}} > 5$ GeV and $17^\circ < \theta^{\tau_{1,2}} < 160^\circ$, was measured to be $\sigma_{\tau\tau}^{\rm kin} = 3.3 \pm 1.3({\rm stat.})^{+1.0}_{-0.7}({\rm syst.})$ pb.

7 Acknowledgments

We appreciate the contributions to the construction and maintenance of the ZEUS detector of many people who are not listed as authors. The HERA machine group and the DESY computing staff are especially acknowledged for their success in providing excellent operation of the collider and data-analysis environment. We thank the DESY directorate for their strong support and encouragement.

References

[1] N. Arteaga-Romero, C. Carimalo and P. Kessler, Z. Phys. **C 52**, 289 (1991).

[2] H1 Coll., A. Aktas et al., Eur. Phys. J. **C 31**, 17 (2003).

[3] H1 Coll., F.D. Aaron et al., Phys. Lett. **B 668**, 268 (2008).

[4] ZEUS Coll., S. Chekanov et al., Phys. Lett. **B 680**, 13 (2009).

[5] H1 and ZEUS Collaborations, F.D. Aaron et al., JHEP **10**, 013 (2009).

[6] H1 Coll., A. Aktas et al., Eur. Phys. J. **C 48**, 699 (2006).

[7] ZEUS Coll., S. Chekanov et al., Phys. Lett. **B 583**, 41 (2004).

[8] ZEUS Coll., U. Holm (ed.), *The ZEUS Detector*. Status Report (unpublished), DESY (1993), available on `http://www-zeus.desy.de/bluebook/bluebook.html`.

[9] N. Harnew et al., Nucl. Inst. Meth. **A 279**, 290 (1989);
B. Foster et al., Nucl. Phys. Proc. Suppl. **B 32**, 181 (1993);
B. Foster et al., Nucl. Inst. Meth. **A 338**, 254 (1994).

[10] A. Polini et al., Nucl. Inst. Meth. **A 581**, 656 (2007).

[11] M. Derrick et al., Nucl. Inst. Meth. **A 309**, 77 (1991);
A. Andresen et al., Nucl. Inst. Meth. **A 309**, 101 (1991);
A. Caldwell et al., Nucl. Inst. Meth. **A 321**, 356 (1992);
A. Bernstein et al., Nucl. Inst. Meth. **A 336**, 23 (1993).

[12] J. Andruszków et al., Preprint DESY-92-066, DESY, 1992;
ZEUS Coll., M. Derrick et al., Z. Phys. **C 63**, 391 (1994);
J. Andruszków et al., Acta Phys. Pol. **B 32**, 2025 (2001).

[13] M. Helbich et al., Nucl. Inst. Meth. **A 565**, 572 (2006).

[14] T. Abe, Comp. Phys. Comm. **136**, 126 (2001).

[15] H. Jung, Comp. Phys. Comm. **86**, 147 (1995).

[16] H. Spiesberger, HERACLES *and* DJANGOH*: Event Generation for ep Interactions at HERA Including Radiative Processes*, 1998, available on `http://www.desy.de/~hspiesb/djangoh.html`.

[17] T. Sjöstrand et al., Comp. Phys. Comm. **135**, 238 (2001).

[18] R. Brun et al., GEANT3, Technical Report CERN-DD/EE/84-1, CERN, 1987.

[19] P.D. Allfrey et al., Nucl. Inst. Meth. **A 580**, 1257 (2007).

[20] J. Maeda, Ph.D. Thesis (unpublished), Tokyo Institute of Technology, 2009.

[21] ZEUS Coll., J. Breitweg et al., Z. Phys. **C 74**, 207 (1997).

[22] S. Catani et al., Nucl. Phys. **B 406**, 187 (1993).

[23] S.D. Ellis and D.E. Soper, Phys. Rev. **D 48**, 3160 (1993).

[24] T. Carli and B. Koblitz, Nucl. Inst. Meth. **A 501**, 576 (2003).

[25] ZEUS Coll., S. Chekanov et al., Eur. Phys. J. **C 44**, 463 (2005).

[26] J.R. Forshaw and M.H. Seymour, JHEP **09**, 009 (1999).

[27] R. Shehzadi, Ph.D. Thesis, University of Bonn, Report BONN-IR-11-01, 2011.

Topology	e-μ	e-e-μ	e-jet	e-e-jet	μ-jet	e-μ-jet	jet-jet	e-jet-jet
Electrons	$N_e = 1$	$N_e = 2$	$N_e = 1$	$N_e = 2$	$N_e = 0$	$N_e = 1$	$N_e = 0$	$N_e = 1$
Muons	$N_\mu = 1$		$N_\mu = 0$		$N_\mu = 1$		$N_\mu = 0$	
Tau jets	$N_{\rm jet} = 0$		$N_{\rm jet} = 1$				$N_{\rm jet} = 2$	
$N_{\rm trk}$	$N_{\rm trk} = 2$	$2 \leq N_{\rm trk} \leq 3$	$2 \leq N_{\rm trk} \leq 7$					
$(E - P_Z)$	< 45 GeV	< 60 GeV	< 45 GeV	< 60 GeV	< 45 GeV	< 60 GeV	< 45 GeV	< 60 GeV
Charge cuts	$Q_e \neq Q_\mu$ $Q_e \neq Q_{\rm beam}$ (if $\theta_e > 1.0$)		$Q_e \neq Q_{\rm jet}$ $Q_{\rm jet} = \pm 1$ $Q_e \neq Q_{\rm beam}$ (if $\theta_e > 1.0$)				$Q_{\rm jet,1} \neq Q_{\rm jet,2}$, $Q_{\rm jet} = \pm 1$	

Table 1: *Definition and selection criteria for each event topology for tau-pair production. The symbols N_e and N_μ refer to the number of selected electrons and muons in the event, $N_{\rm jet}$ indicates the number of tau-candidate jets. The selection criteria and other variables are defined in the text.*

ZEUS ditau events HERA II data (L=0.33 fb^{-1})

Topology	(e-)e-μ	(e-)e-jet	(e-)μ-jet	(e-)jet-jet	Total
Data	4	7	4	10	25
Total MC	$3.6^{+1.3}_{-0.3}$	$8.8^{+1.8}_{-0.8}$	$8.0^{+2.2}_{-1.2}$	$14.4^{+2.2}_{-3.5}$	$34.8^{+3.9}_{-3.8}$
$\tau^+\tau^-$ MC	$3.0^{+0.3}_{-0.2}$	$5.3^{+0.3}_{-0.2}$	$5.9^{+0.5}_{-0.5}$	$9.0^{+0.4}_{-0.3}$	$23.2^{+0.7}_{-0.7}$

Table 2: *The observed and predicted ditau-event yields for the sum of the topologies and for each channel separately. The total MC expectations include the sum due to ditau production, DIS neutral current interactions, photoproduction events and dielectron/dimuon pair production. The experimental systematic uncertainties are quoted on the MC expectations.*

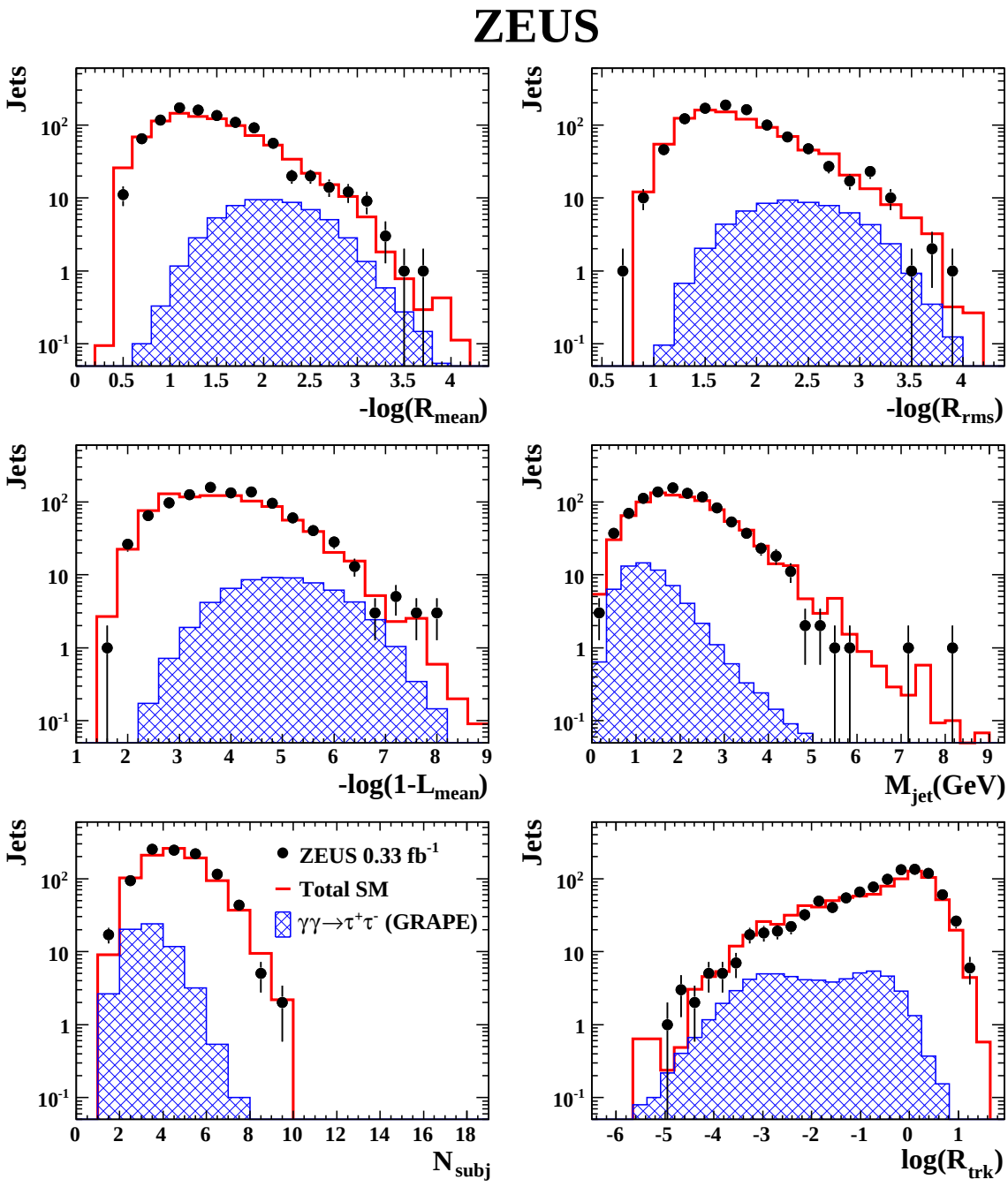

Figure 1: *Distributions of the variables used for the tau-jet discriminant, for the data (dots) and the sum of the MC expectations (solid line), after all selection criteria except for the discriminant cut. The variables are defined in the text. The data are shown with the statistical uncertainty (vertical error bars). The contribution of the ditau signal as predicted by* GRAPE *is shown separately (hatched histogram). The background due to photoproduction interactions is normalised with the procedure described in the text. The other MC expectations are normalised to the luminosity of the data.*

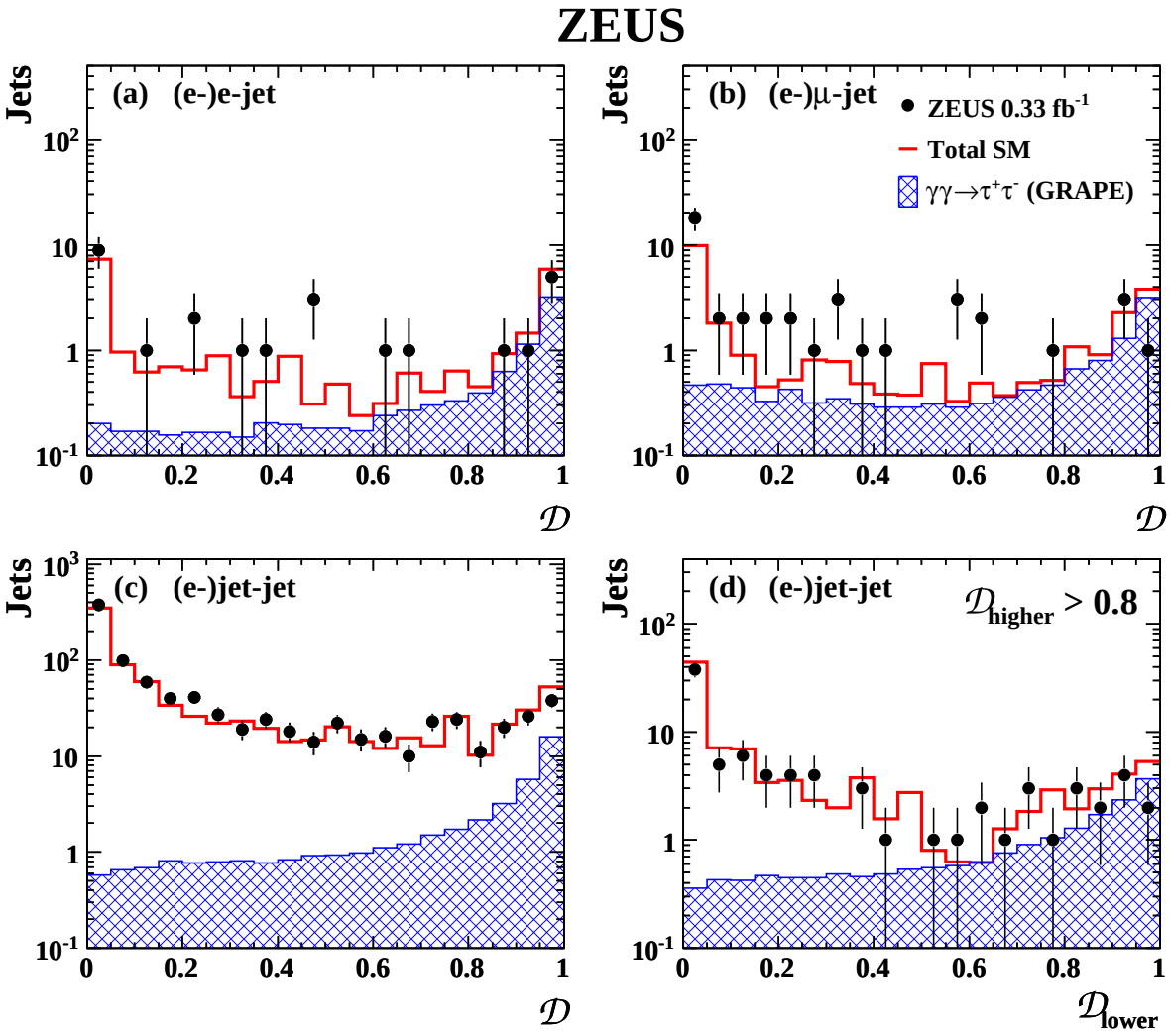

Figure 2: *Tau-jet discriminant values for the three decay topologies (a) (e-)e-jet, (b) (e-)μ-jet and (c) (e-)jet-jet for the events after all selection criteria, except the discriminant cut. For the (e-)jet-jet channel, (d) shows the discriminant distribution for the jet with lower $\mathcal{D}$ value, after the requirement $\mathcal{D} > 0.8$ for the jet with higher $\mathcal{D}$. Other details as in the caption to Fig. 1.*

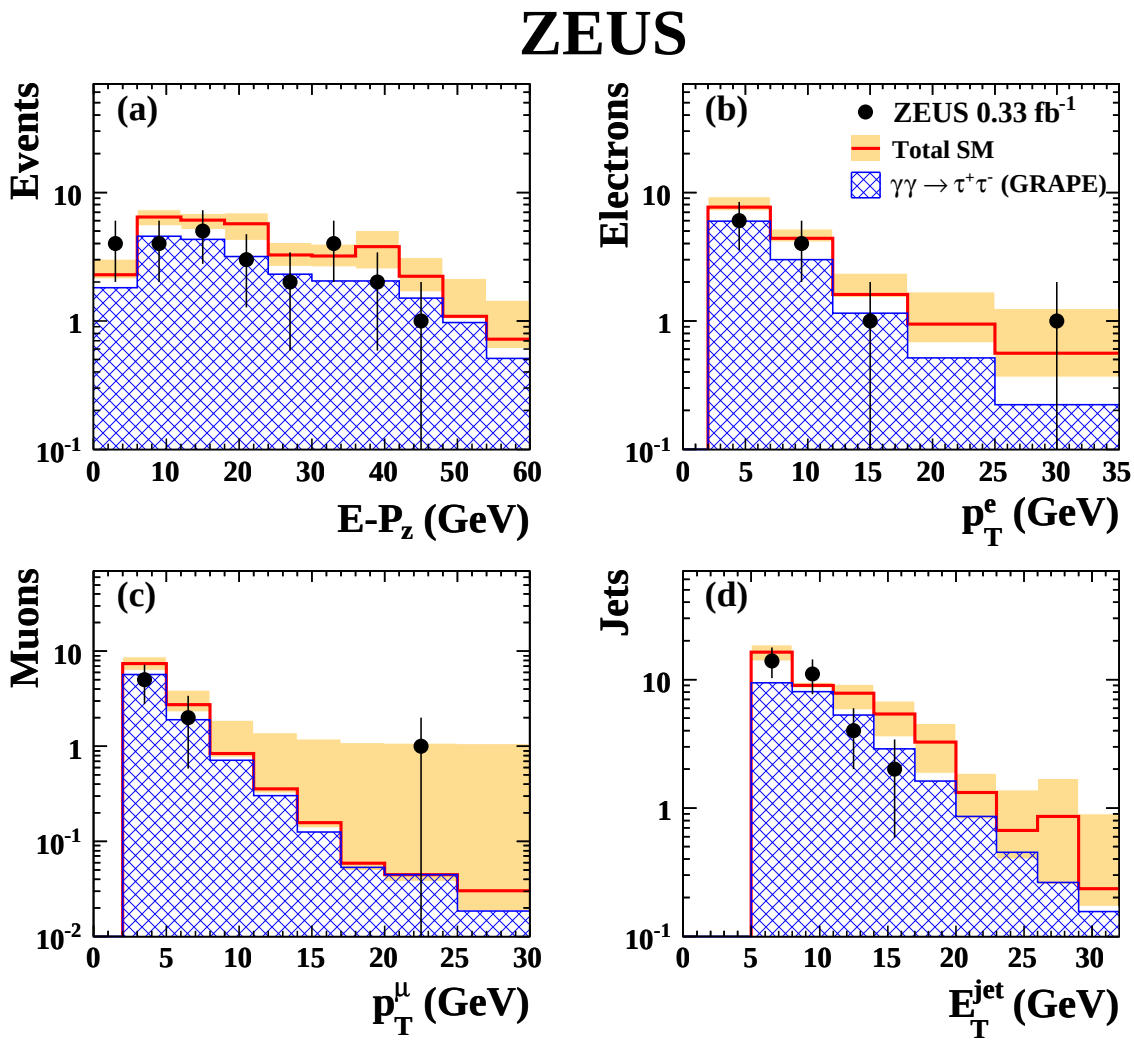

Figure 3: *Distributions of the selected events compared with the predictions from the Standard Model (SM). The plots show: (a) the variable $E - P_Z$, (b) the transverse momentum, p_T^e, of the electrons, (c) the transverse momentum, p_T^μ, of the muons and (d) the transverse energy of each jet, E_T^{jet}. The shaded bands show the systematic uncertainty on the SM expectation. Other details as in the caption to Fig. 1.*

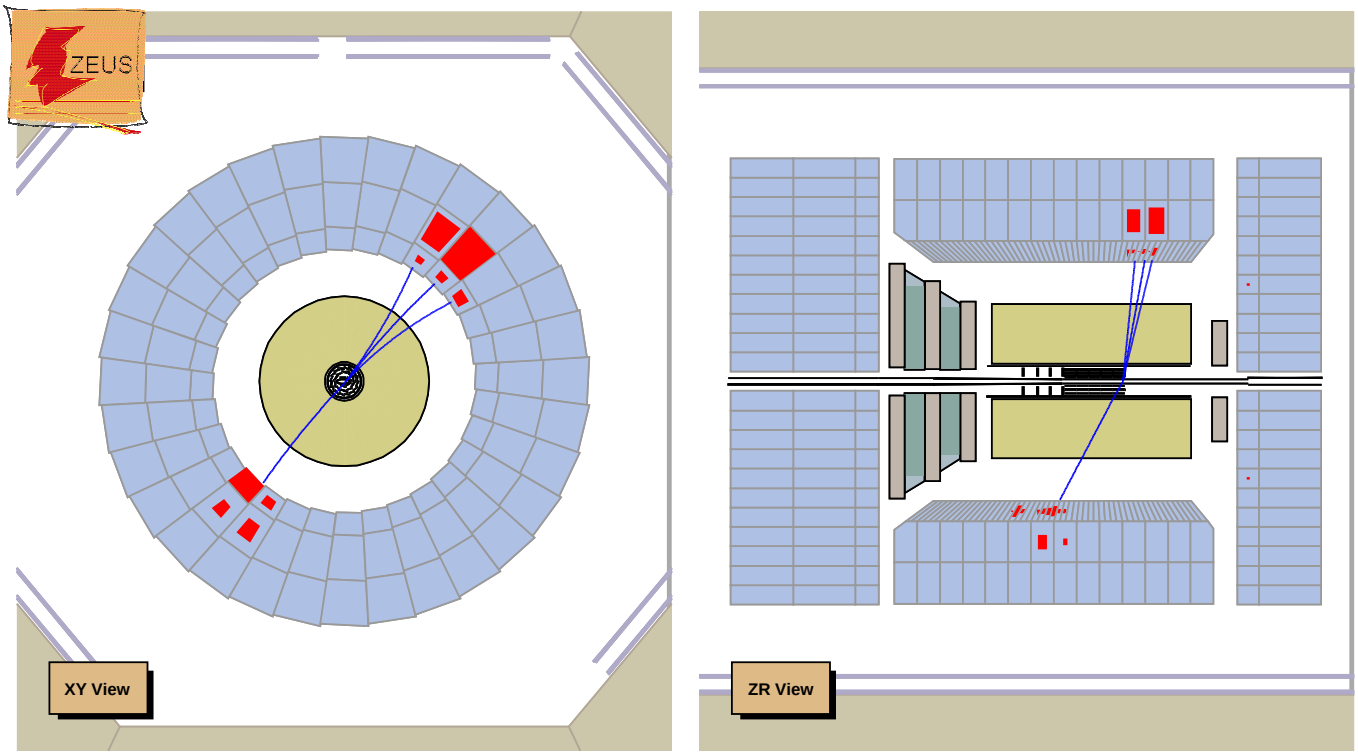

Figure 4: *Event display of a data event selected in the jet-jet channel. One jet has one charged track, the other jet has three charged tracks. The two jets have* $E_T^{\mathrm{jet1}} = 7.8$ GeV *and* $E_T^{\mathrm{jet2}} = 6.9$ GeV *and the visible mass is* $M_{\tau\tau}^{\mathrm{visible}} = 15.6$ GeV.

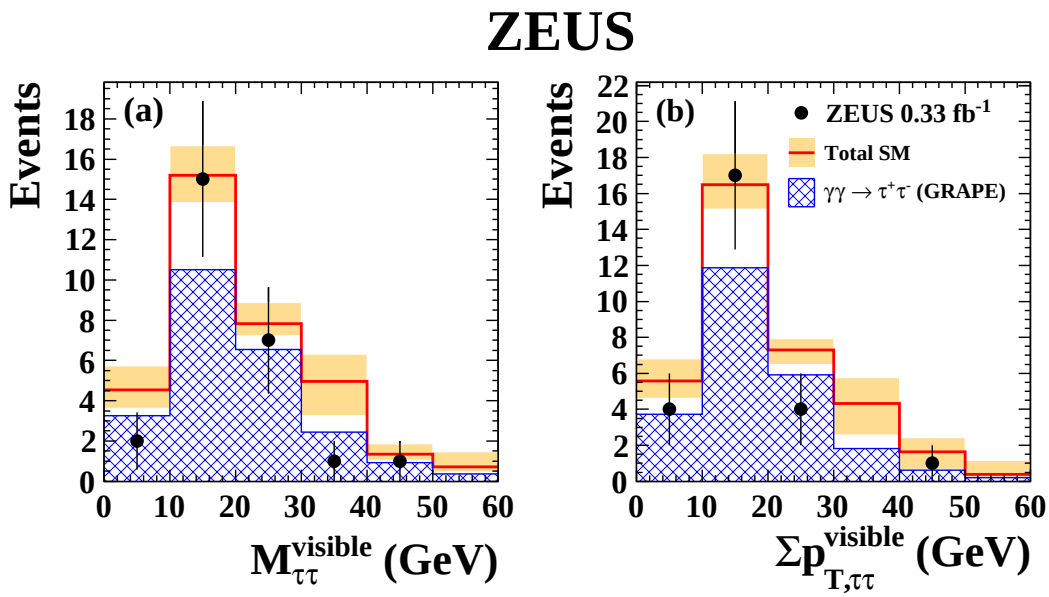

Figure 5: *Distributions of the events after all selection cuts as a function of (a) the visible invariant mass of the tau pair, $M_{\tau\tau}^{\rm visible}$, and (b) the scalar sum of the transverse momenta of the two tau candidates, $\sum p_{T,\tau\tau}^{\rm visible}$. The selected e-e-jet event has two entries in the plots, one for each electron-jet combination. The data (dots) are compared with the predictions of the sum of the Monte Carlo expectations and to the ditau MC only. The shaded bands show the systematic uncertainty on the SM expectation.*